Generalized Hamiltonian of mean-force approach to open quantum systems coupled to finite baths in thermoequilibrium

Xuerui Du,[1] Jianhui Wang,[1,2,*] and Yongli Ma[1,†]
[1]*State Key Laboratory of Surface Physics and Department of Physics, Fudan University, Shanghai 200433, China*
[2]*Department of Physics, Nanchang University, Nanchang 330031, China*

(Received 5 September 2024; accepted 30 January 2025; published 24 February 2025)

The prevailing method for addressing strong-coupling thermodynamics typically involves open quantum systems coupled to infinite baths in equilibrium through the Hamiltonian of mean force (HMF). However, its applicability to finite baths remains limited. In this work, we transcend this limit by considering the impacts of system-bath coupling which is not only on the system but also on the finite bath feedback. When the bath and system sizes are comparable, they act as each other's effective 'bath'. We introduce a parameter α within [0, 1], where α and $1-\alpha$ act as weighting factors to distribute the system-bath coupling between the system and the bath. Our approach innovatively incorporates the effect of coupling on the respective effective 'bath' into both the system and bath in the statistical factor form. We generalize the HMF and propose quantum Hamiltonians of mean forces to handle the distributed coupling of the system to finite baths. The additional parameter α is determined by minimizing the joint free energy density and is a new thermodynamic quantity representing the finite bath's influence. Examining the damped quantum harmonic oscillator with a finite bath, we find that α affects both states, leading to a complex phase diagram with unique phenomena at critical temperatures T_L and T_R, including valleys, peaks, negative values, and discontinuities in entropy and specific heat. Notably, these anomalies disappear when $\alpha \to 1$, both at high temperatures and in the thermodynamic limit, indicating the negligible influence of coupling on the bath states and reverting to the HMF. Thus, studying finite-sized baths holds substantial significance in small quantum systems.

DOI: 10.1103/PhysRevE.111.024139

I. INTRODUCTION

Extensive research has been conducted on open quantum systems coupled to infinite baths. The development of strong coupling thermodynamics has emerged as a prominent focus in recent decades [1–10]. While the statistical foundation of thermodynamics has been successfully applied across various fields, its applicability faces challenges with decreasing sizes of composite systems, particularly in the nanoscale and quantum systems [2,11,12]. At the nanoscale, the surface-to-volume ratio increases significantly, rendering the assumption that system-bath interactions are negligible compared to the system's thermal energy invalid. The effects of size and quantum come into play, necessitating the development of new theoretical frameworks by the roots to better understand and describe such open systems.

The Hamiltonian of mean force (HMF) is a useful tool for decoupling small systems in thermo-equilibrium with a heat bath [1,5,13]. This approach assumes that the bath remains in its bare state and the partition function of the reduced system is derived from the ratio of the total partition function to that of the bare bath. Existing research primarily explores dynamics through generalized Langevin equations [14,15], completely positive and trace-preserving (CPTP) maps [6], thermofield dynamics [16], Lindblad master equations [9,17–19], or eigenstate thermalization hypothesis [20–22], but the thermodynamics of systems coupled to finite baths are largely unexamined.

Here, we provide a general thermodynamic framework to describe this open quantum system with arbitrary coupling to a finite bath in equilibrium by extending the HMF to a pair of quantum Hamiltonians of mean forces (QHMFs). In this framework, the system and bath are treated as each other's effective "bath" at the quantum level. We introduce the parameter α, analogous to the additional parameter proposed by Hilt for nano-systems [23], and use α and $1-\alpha$ to quantify the distribution of the interaction in the system and the bath respectively, due to the system-bath coupling within a fully quantum framework, treating the equilibrium states of both the system and the bath equivalently. Constrained by coupling strength, temperature, and the number of bath modes, the distribution is determined by minimizing the joint free energy density. We then observe the rich behaviors of α across different coupling and bath modes regimes, resulting in six distinct phases, as shown in Fig. 1. Notably, phases C and D exhibit entropy discontinuities not observed in traditional HMF approaches. Unlike the HMF, where the system-bath coupling does not give feedback to the baths, our method only converges to this allocation in the baths' thermodynamic limit (TL), as demonstrated in classical scenarios [24]. This approach opens new avenues for exploring the thermodynamics of small quantum systems.

*Contact author: wangjianhui@ncu.edu.cn
†Contact author: ylma@fudan.edu.cn

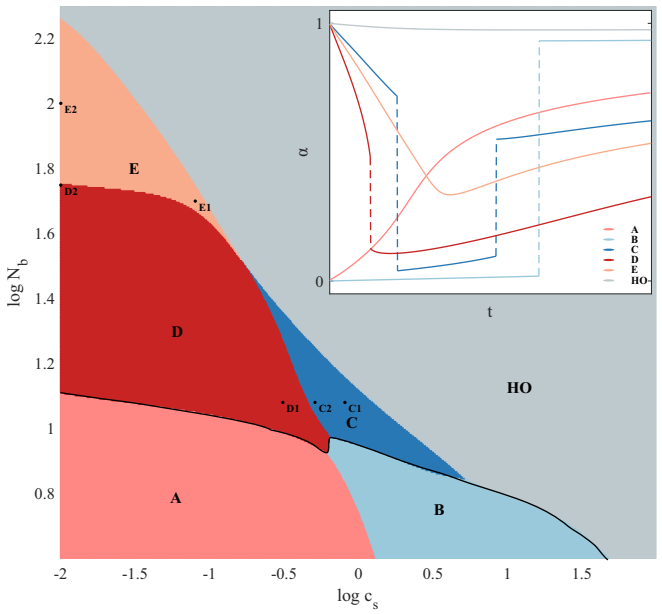

FIG. 1. Phase diagram of the system of interest: The heat bath mode numbers N_b versus the effective coupling strength c_s are plotted on a base-10 logarithmic scale along both coordinate axes. The diagram reveals six phases, corresponding to six types of $\alpha - t$ relationships. (Inset: Schematic diagrams are depicted qualitatively. The perpendicular dashed lines indicate jumps). The six identified phases are labeled as P = A, B, C, D, E, and HO (free harmonic oscillators). We set $\bar{\omega}_D = 1000$ for this analysis. Phases A and B, occurring below the solid black line where N_b is small, are considered non-physical due to their inconsistency with the third law of thermodynamics. Points labeled as Pi with i = 1, 2 represent two specific points within phase P. The corresponding temperature-dependent curves of thermodynamic quantities, given specific values of (c_s, N_b), exhibit unique behaviors in each phase (discussed further in the text).

We apply QHMFs to a damped quantum harmonic oscillator, a common model in the open system research [19,25–28], characterized by the Caldeira-Leggett (CL) model [29–31]. While the bath's influence is typically described by its spectral function in the continuum limit [32], we explore the effects of finite baths by discretizing the coupling constants [33]. We aim to uncover novel phenomena, such as valleys, peaks, negative values, and discontinuities in the entropy and specific heat of the system. Some of these anomalies have been observed in dissipative quantum systems [34], fermions interacting with gapless bosons at a quantum-critical point in metals [35], and in the two-level fluctuator-oscillator model [7]. Additionally, our framework can describe cavity spintronics by considering a single bath mode with repulsion [36,37].

The plan of the paper is the following: In Sec. II, we address the theoretical framework of QHMFs. We employ our method to study the CL model of an open quantum system with finite bath in Sec. III, and to reveal the emergence of some novel thermodynamic characteristics at low temperatures for finite baths in Sec. IV. In Sec. V, we discuss the results. In Sec. VI, we conclude the work.

II. THE THEORETICAL FRAMEWORK OF QUANTUM HAMILTONIAN OF MEAN FORCES

A. The total Hamiltonian and HMF

For a general quantum system of interest, denoted by the subscript (s), that is strongly coupled to its bath, denoted by the subscript (b), both are in equilibrium and immersed in a larger environment at an inverse temperature $\beta = 1/k_B T$. The total Hamiltonian is written by

$$\hat{H}_{tot} = \hat{H}_s + \hat{H}_b + \hat{H}_{int}, \tag{1}$$

where $\hat{H}_s$ is an interested system Hamiltonian, $\hat{H}_b$ is the bath Hamiltonian depicts the surrounding particles coupled to the system, and $\hat{H}_{int}$ represents the interaction Hamiltonian between the system and the bath. We extend the traditional concept of slow degrees of freedom, which typically applies only to the system, to include the composite system (the system of interest plus the finite bath), while the fast degrees of freedom are left to the thermostat (a larger environment supplying T). As usual, we neglect the interaction between the total system and the large environment.

When the system-bath coupling is negligible, the reduced density operators of the system and the bath are the standard thermodynamic statistics, i.e. $\hat{\rho}_\nu = e^{-\beta\hat{H}_\nu}/Z_\nu$, where $Z_\nu = \mathrm{Tr}_\nu e^{-\beta\hat{H}_\nu}$ are the partition functions of the bare system (ν = s) and bath (ν = b), respectively. When the coupling is significant, the previous works have defined the HMF to depict the reduced density operator of the system,

$$\hat{\rho}_s = \mathrm{Tr}_b e^{-\beta\hat{H}_{tot}}/Z_{tot}, \tag{2}$$

where $Z_{tot} = \mathrm{Tr}_{tot} e^{-\beta\hat{H}_{tot}}$ is the partition function of the total system. The symbols $\mathrm{Tr}_{tot}, \mathrm{Tr}_s, \mathrm{Tr}_b$ denote the trace over the degrees of freedom of the total system, and the partial traces over the degrees of freedom of the system and the bath, respectively. When the coupling must be taken into consideration, the usual reduced density matrix of the system is proportional to the "renormalized Boltzmann factor"

$$\mathrm{e}^{-\beta\hat{H}_s^*} = \mathrm{Tr}_b \mathrm{e}^{-\beta\hat{H}_{tot}}/Z_b, \tag{3}$$

with $Z_{tot} = Z_s^* Z_b$ and $Z_s^* = \mathrm{Tr}_s e^{-\beta\hat{H}_s^*}$. Here, $\hat{H}_s^*$ is referred to as the HMF, an effective reduced Hamiltonian of the system.

B. QHMFs formula and partition functions

In quantum systems, exact decoupling from the bath is impossible without solving the problem within the combined system and bath Hilbert spaces, particularly in infinite-dimensional cases. The HMF is a key concept (or approximation method) in studying open systems in canonical equilibrium with their environment. When solving the HMF, the information about the heat bath is effectively erased, as the interaction is absorbed into the effective system. This approach is valid when there is a significant disparity in particle numbers between the system and the bath. However, when the system and bath have comparable particle numbers, the effect of coupling on the bath becomes non-negligible.

In finite baths, the system-bath coupling significantly impacts the bath, which cannot be ignored. When the bath size is comparable to the system, each can be treated as the

effective 'bath' of the other, creating complex interdependencies. To quantify this interaction, we introduce a parameter α within the range [0, 1], where α reflects the distribution of the interaction on the bath, and $1-\alpha$ on the system. This dual-parameter approach provides a nuanced understanding of finite-size baths, where traditional approximations of the total system fail. The effective 'bath' Hamiltonians for the system and bath are defined as follows:

$$\hat{H}_{\rm b}^{\alpha} = \hat{H}_{\rm b} + (1-\alpha)\hat{H}_{\rm int}, \tag{4a}$$

$$\hat{H}_{\rm s}^{\alpha} = \hat{H}_{\rm s} + \alpha\hat{H}_{\rm int}. \tag{4b}$$

We treat the system and bath symmetrically by tracing out the bath (or system) information equivalently, even within certain approximation methods. This approach allows us to derive generalized HMF for the system (or bath). In the special case of $\alpha = 1$, these Hamiltonians correspond to a decoupled scenario, where the coupling does not affect the effective 'bath' Hamiltonian $\hat{H}_{\rm b}^{\alpha}$ for the system, which is equivalent to the bare bath.

Based on these effective Hamiltonians (4), we can extend the usual HMF to QHMFs and express them in the Boltzmann factor forms $\mathrm{e}^{-\beta\hat{H}^{*}_{\rm s,b}}$. In more detail, they are the form

$$\mathrm{e}^{-\beta\hat{H}^{*}_{\rm s}} = \left(\mathrm{Tr_b e}^{-\beta\hat{H}^{\alpha}_{b}}\right)^{-1}\mathrm{Tr_b e}^{-\beta\hat{H}_{\rm tot}}, \tag{5a}$$

$$\mathrm{e}^{-\beta\hat{H}^{*}_{\rm b}} = \left(\mathrm{Tr_s e}^{-\beta\hat{H}^{\alpha}_{s}}\right)^{-1}\mathrm{Tr_s e}^{-\beta\hat{H}_{\rm tot}}. \tag{5b}$$

It is worth noting that every term in Eq. (5), despite undergoing the trace operation and approximations, remains an operator. The exponent -1 applied to the operator indicates taking its inverse. At the quantum level, these prefactors are operators, while in HMF they return to partition functions. The key point is that in QHMFs, the density operator for systems or baths is proportional to $e^{-\beta\hat{H}^{*}_{\nu}}$, rather than $e^{-\beta\hat{H}^{\alpha}_{\nu}}$, where the latter represents the effective 'bath'. Besides, Eq. (5) represents the unnormalized Gibbs state of the real physical system and bath since it is derived by tracing out the bath and system degrees of freedom respectively.

Our approach innovatively incorporates the effect of coupling by introducing the effective 'bath' for both the system and bath in Boltzmann factor in our model. For small coupling strengths or high temperatures, methods such as Trotter decomposition [38] or the Baker-Campbell-Hausdorff (BCH) formula can be used. But for arbitrary coupling and temperature, it seems like an intractable problem to calculate the QHMFs even the associated thermodynamic quantities. Nevertheless, the partition function $Z^{*}_{\rm s,b}$ is fundamental, simplifies to a manageable form through the trace in Eq. (5), and is then used to calculate the free energy. After performing partial traces Tr_{ν} in Eq. (5) for the bare system and bath with $\nu = \mathrm{s}$ and $\nu = \mathrm{b}$, respectively, we obtain

$$Z^{*}_{\nu} = \mathrm{Tr}_{\nu} e^{-\beta\hat{H}^{*}_{\nu}}. \tag{6}$$

Thus, all thermodynamic quantities can be derived from these reduced partition functions for $\nu = \mathrm{s}$ and b.

C. Thermodynamic quantities and additional parameter α

In the strong coupling regime, the definition of thermodynamic quantities is ambiguous [2,24,39]. One approach follows the traditional statistical definitions of thermodynamics [24], while another maintains thermodynamic relations [3]. These two approaches are inconsistent in strongly coupled quantum systems but converge as the coupling approaches zero. The second approach naturally satisfies thermodynamic relations without relying on the von Neumann entropy to define thermodynamic entropy. It is known that in unitary systems, von Neumann entropy and thermodynamic entropy are contradictory, as von Neumann entropy remains constant, whereas the second law of thermodynamics requires $\delta S \geqslant 0$ [40]. We believe that the thermodynamic relations are universal and the entropy awaits for approaching further. Thus, we adopt the fundamental thermodynamic relations for the reduced system and bath. Based on the QHMFs, the interested system and bath are completely separated. Within the canonical ensemble with the thermodynamic variables (N_{ν}, V_{ν}, T), the free energy for the decoupled system ($\nu = \mathrm{s}$) and bath ($\nu = \mathrm{b}$) can be expressed in the following form: (in brief, we define $k_{\rm B} = \hbar = 1$ hereafter)

$$F^{*}_{\nu} = -T \ln Z^{*}_{\nu}. \tag{7}$$

The entropy, internal energy, and specific heat are taken from the reduced formulas

$$S^{*}_{\nu} = -\frac{\partial F^{*}_{\nu}}{\partial T}, \quad E^{*}_{\nu} = -\frac{\partial \ln Z^{*}_{\nu}}{\partial \beta}, \quad C^{*}_{V_{\nu}} = \frac{\partial E^{*}_{\nu}}{\partial T}. \tag{8}$$

Obviously, they obey the fundamental thermodynamic relations $F^{*}_{\nu} = E^{*}_{\nu} - TS^{*}_{\nu}$ for the reduced system and bath. Additional parameter α is determined by minimizing the reduced total free energy density $f^{*}_{\rm tot}$,

$$\alpha = \arg\min_{\alpha} f^{*}_{\rm tot} = \arg\min_{\alpha}(f^{*}_{\rm s} + f^{*}_{\rm b}). \tag{9}$$

Where $f^{*}_{\nu} = F^{*}_{\nu}/N_{\nu}$. α will depend on the temperature and the parameters of the total system. Since the thermodynamic quantities represented by Q involve partial derivatives concerning temperature that include α, the calculation requires using:

$$\frac{\partial Q}{\partial T} = \left(\frac{\partial Q}{\partial T}\right)_{\alpha} + \left(\frac{\partial Q}{\partial \alpha}\right)_{T}\frac{\partial \alpha}{\partial T}. \tag{10}$$

Thus the thermodynamic quantities expressed on Eq. (7) and Eq. (8) sensitively depend on α and its derivatives concerning temperature. This constitutes our theoretical framework, which we will apply to an interesting coupled quantum system.

III. QHMFs FOR A DAMPED QUANTUM OSCILLATOR

A. CL model

The CL model commonly uses the study for a damped quantum oscillator for the total Hamiltonian,

$$\hat{H}_{\rm tot} = \frac{\hat{P}^2}{2M} + \frac{1}{2}M\Omega^2\hat{Q}^2 + \sum_{j=1}^{N_{\rm b}}\left[\frac{\hat{p}_j^2}{2m_j} + \frac{m_j\omega_j^2}{2}\left(\hat{q}_j - \frac{C_j}{m_i\omega_j^2}\hat{Q}\right)^2\right]. \tag{11}$$

Dividing the above Hamiltonian into the form of Eq. (1), the first term

$$\hat{H}_{\rm s} = \frac{\hat{P}^2}{2M} + \frac{1}{2}M\Omega^2\hat{Q}^2 + \sum_{j=1}^{N_{\rm b}} \frac{C_j^2}{2m_j\omega_j^2}\hat{Q}^2 \tag{12}$$

is the Hamiltonian of the system described by a quantum oscillator with mass M and frequency Ω and the last term is the coupling-induced trapping potential which is the renormalized term to keep the bath passive in TL [41]. The second term

$$\hat{H}_{\rm b} = \sum_{j=1}^{N_{\rm b}} \left(\frac{\hat{p}_j^2}{2m_j} + \frac{1}{2}m_j\omega_j^2\hat{q}_j^2 \right) \tag{13}$$

depicts the bath consisting of $N_{\rm b}$ oscillators with mass m_j and frequency ω_j respectively. The bath frequency spectrum for the bath mode $j = 1, 2, \ldots, N_{\rm b}$ is $\omega_j = \Lambda_j\omega_{\rm D}$ within the cut frequency $\omega_{\rm D}$. There are two kinds of bath frequency distributions, one is equidistant $\Lambda_j = j/N_{\rm b}$ and the other is dense in the low frequencies $\Lambda_j = \Lambda^{j-N_{\rm b}}$, where $\Lambda > 1$ and we take $\Lambda = 2$ [42]. The last linear coupling of the system and bath in the displacement is written by

$$\hat{H}_{\rm int} = -\sum_{j=1}^{N_{\rm b}} C_j\hat{Q}\hat{q}_j. \tag{14}$$

Here, C_j is the coupling constant in the form [32,33]

$$C_j = \sqrt{\frac{2}{\pi}\gamma M m_j\omega_j^2\Delta_j\frac{\omega_{\rm D}^2}{\omega_j^2+\omega_{\rm D}^2}}, \tag{15}$$

which obeys a Drude-Ullersma spectrum with a damping coefficient γ. Here, we define the jth bath frequency difference as $\Delta_j = |\omega_j - \omega_{j-1}| = \delta_j\omega_{\rm D}$ for $j \geqslant 2$. Two types of bath frequency distributions are considered: $\delta_j = N_{\rm b}^{-1}$ and $\delta_j = (1-1/\Lambda)\Lambda^{j-N_{\rm b}}$. For $j = 1$, we set $\omega_0 = 0$ and $\delta_1 = \Lambda^{1-N_{\rm b}}$ for the second type of bath frequency. In the continuum limit as $N_{\rm b} \to \infty$, $\Delta_{N_{\rm b}} \to 0$ for the first type of bath frequency, and $\Lambda = 1$ ensures $\Delta_j = 0$ for the second type within the numerical renormalization group framework [42]. In numerical calculations of the discrete model, however, by selecting Λ in the [1.8, 3.0] range and extrapolating to $\Lambda = 1$, the results align with renormalization group theory's prediction. Moreover, selecting $\Lambda = 2$ shows that the results remain robust and consistent, even with slight variations. In the continuum spectrum, the spectral density function is Ohmic [33]. For a finite bath, i.e., a finite number of $N_{\rm b}$, choosing the second type of bath frequency is appropriate to weigh different energy scales, especially emphasizing low-energy contributions properly.

B. QHMFs

To derive the expressions for the QHMFs in a quantum open system consisting of a damped quantum oscillator in equilibrium coupled to a finite bath, we proceed as follows based on Eq. (4) and Eq. (5). First, to obtain the prefactors (operators) of the QHMFs, we shift the position of the jth bath particle, denoted as $\hat{\tilde{q}}_j$, relative to the system position: $\hat{\tilde{q}}_j = \hat{q}_j - (1-\alpha)C_j\hat{Q}/m_j\omega_j^2$. Similarly, we shift the system position relative to the jth bath particle as $\hat{\tilde{Q}} = \hat{Q} - \alpha N_{\rm b}C_j\hat{q}_j/M\bar{\Omega}^2$, where $\bar{\Omega}^2 = \Omega^2 + \sum_{j=1}^{N_{\rm b}}\frac{C_j^2}{Mm_j\omega_j^2}$. On the other hand, we employ semi-classical approximations for the operators of QHMFs in Eq. (5), where the Hamiltonian is approximated by treating quantum operators as classical variables during the tracing process, due to the complexity of performing exact tracing. However, the trace results are subsequently treated as operators, with their noncommutativity explicitly accounted for in the final calculations. Here, the shifts in $\mathrm{Tr}_{\rm b,s}e^{-\beta\hat{H}_{\rm tot}}$ are given by $\hat{\tilde{q}}_j = \hat{q}_j - C_j\hat{Q}/m_j\omega_j^2$ and $\hat{\tilde{Q}} = \hat{Q} - N_{\rm b}C_j\hat{q}_j/M\bar{\Omega}^2$, which are similar to the shifts used for the prefactor but with $\alpha = 0, 1$. Note that the heat bath statistic average $\langle\hat{q}_j\hat{q}_{j'}\rangle_{\rm b} = 0$ for $j \neq j'$, we have a pair of QHMFs in the forms

$$e^{-\beta\hat{H}_{\rm s}^*} = e^{-\beta\hat{h}_{\rm s}^\alpha}e^{-\beta(\hat{H}_{\rm s}-\hat{h}_{\rm s}^0)}, \tag{16a}$$

$$e^{-\beta\hat{H}_{\rm b}^*} = e^{-\beta\hat{h}_{\rm b}^\alpha}e^{-\beta(\hat{H}_{\rm b}-\hat{h}_{\rm b}^1)}. \tag{16b}$$

Here, $\hat{h}_{\rm s}^\alpha = (1-\alpha)^2\sum_{j=1}^{N_{\rm b}}\frac{C_j^2}{2m_j\omega_j^2}\hat{Q}^2 = (1-\alpha)^2c_sM\Omega^2\hat{Q}^2$ for the system, and $\hat{h}_{\rm b}^\alpha = \sum_{j=1}^{N_{\rm b}}\hat{h}_{{\rm b}j}^\alpha$ with $\hat{h}_{{\rm b}j}^\alpha = \alpha^2\frac{C_j^2}{2M\bar{\Omega}^2}\hat{q}_j^2 = \alpha^2\frac{c_j}{2}m_j\omega_j^2\hat{q}_j^2$ for the jth bath mode. They are all $\alpha-$dependent coupling Hamiltonians. We have used the dimensionless parameters

$$c_{\rm s} = \frac{\gamma}{\pi\Omega^2}\sum_{j=1}^{N_{\rm b}}\frac{\Delta_j\omega_{\rm D}^2}{\omega_j^2+\omega_{\rm D}^2} = \frac{\omega_{\rm D}\gamma}{\pi\Omega^2}\sum_{j=1}^{N_{\rm b}}\frac{\delta_j}{1+\Lambda_j^2}, \tag{17a}$$

$$c_j = \frac{2\gamma}{\pi\Omega^2(1+2c_{\rm s})}\frac{\Delta_j\omega_{\rm D}^2}{\omega_{\rm D}^2+\omega_j^2} = \frac{2\omega_{\rm D}\gamma}{\pi\Omega^2(1+2c_{\rm s})}\frac{\delta_j}{1+\Lambda_j^2}, \tag{17b}$$

Here, $c_{\rm s}$, representing the effective coupling strength, characterizes the interaction intensity between the system and the bath. It is important to emphasize that while $c_j \to 0$ as $N_{\rm b} \to \infty$ due to $\delta_j \to 0$, $c_{\rm s}$ may still remain finite. Given that the Gibbs state of the system (or bath) is characterized by Gaussian distributions, the partition function of the system s (or bath b) can be evaluated using Isserlis' theorem as

$$Z_{\rm s}^* = \frac{1}{2\sinh\frac{1}{2}\beta\Omega}\frac{1}{\sqrt{1+y_{\rm s}}}, \tag{18a}$$

$$Z_{\rm b}^* = \prod_{j=1}^{N_{\rm b}}\frac{1}{2\sinh\frac{1}{2}\beta\bar{\omega}_j}\frac{1}{\sqrt{1+y_j}}. \tag{18b}$$

Here, $y_{\rm s} = (1-\alpha)^2c_{\rm s}\beta\Omega\coth\frac{1}{2}\beta\Omega$, $y_j = \frac{1}{2}\alpha^2\frac{c_j}{1-c_j}\beta\bar{\omega}_j\coth\frac{1}{2}\beta\bar{\omega}_j$, and $\bar{\omega}_j = \omega_j\sqrt{1-c_j}$. These results are valid only for distinguishable particles with $(N_{\rm s}, N_{\rm b})$, and the exact partition function has been detailed in [43]. Notably, $\bar{\omega}_j$ remains a real number, as c_j never exceeds 1. This is ensured by the requirement that the sum $\sum_{j=1}^{N_{\rm b}}c_j = \frac{2c_{\rm s}}{1+2c_{\rm s}}$ is always less than 1, even as a function of $N_{\rm b}$ and $\omega_{\rm D}\gamma$. When $c_{\rm s} \propto \gamma \to 0$, the system and bath revert to the model of free harmonic oscillators. Similarly, as $N_{\rm b} \to \infty$, the partition function of the bath reverts to the results of a series of bare modes owing to $c_j \to 0$.

With the details of the model established, we first consider the physical parameters, including the environment temperature T, damping coefficient γ, and cutoff frequency $\omega_{\rm D}$ (all in

units of the quantum oscillator frequency Ω), as well as the number of bath modes N_b. The reduced total free energy density, as a function of the dimensionless parameters $t = T/\Omega$, $\bar{\gamma} = \gamma/\Omega$, $\bar{\omega}_\mathrm{D} = \omega_\mathrm{D}/\Omega$, N_b, and α, is given by:

$$f^*_\mathrm{tot} = T\left[\ln 2\sinh\frac{1}{2}\beta\Omega + \frac{1}{2}\ln(1+y_\mathrm{s})\right] + \frac{T}{N_\mathrm{b}}\sum_{j=1}^{N_\mathrm{b}}\left[\ln 2\sinh\frac{1}{2}\beta\bar{\omega}_j + \frac{1}{2}\ln(1+y_j)\right]. \quad (19)$$

To find the extremum of the function with respect to α, we derive the condition that α must satisfy:

$$\frac{1-\alpha}{(1-\alpha)^2\beta\Omega + \frac{1}{c_\mathrm{s}}\tanh\frac{1}{2}\beta\Omega} = \frac{1}{N_\mathrm{b}}\sum_{j=1}^{N_\mathrm{b}}\frac{\alpha}{\alpha^2\beta\Omega + 2\left(\frac{1}{c_j}-1\right)\frac{\Omega}{\bar{\omega}_j}\tanh\frac{1}{2}\beta\bar{\omega}_j}. \quad (20)$$

Thus, α is a function of t, $\bar{\omega}_\mathrm{D}$, c_s, and N_b. Moreover, it must satisfy the condition $\frac{\partial^2 f^*_\mathrm{tot}}{\partial\alpha^2} > 0$ to ensure a minimum. Given that ω_D is typically fixed in practice, we select appropriate values for $\bar{\omega}_\mathrm{D}$ and vary the reduced temperature t and the total system parameters c_s and N_b.

C. Phase diagram and critical behaviors

From Eq. (20), we identify six distinct types of $\alpha - t$ relationships, each corresponding to different physical regimes. The inset of Fig. 1 illustrates the schematic diagrams of the six types of α vs t curves, each qualitatively describing the behavior within specific parameter ranges. These are referred to as six phases due to their distinct thermodynamic behaviors. The behavior within each phase leads to quantitative changes in thermodynamic quantities, whereas its behavior across different phases results in qualitative changes in these quantities. By considering Eqs. (15) and (17a), we introduce the effective coupling strength c_s in our model as a replacement for the microscopic coupling strength C_j and the macroscopic damping coefficient γ. Notably, while the phase diagram is plotted as $\log N_\mathrm{b}$ vs $\log c_\mathrm{s}$, each region distinctly represents a specific type of $\alpha - t$ relationship. These regions, labeled A, B, C, D, E, and free harmonic oscillator (HO), exhibit various thermodynamic behaviors that define the different phases of the system.

Following the detailed calculations (outlined below), we derive the quantitative six-phase diagrams. The calculations reveal that α exhibits complex behavior across different parameter ranges, resulting in distinct thermodynamic properties across the various phases. In our numerical calculations, the extreme values of the dimensionless parameter $\xi = T\frac{\partial\alpha}{\partial T}$, which represents the temperature-scaled slope of α, indicate the occurrence of a critical temperature. Specifically, a critical temperature is suggested when $|\xi| \geqslant 0.3$. This is observed both in systems with a small number of N_b due to finite-size effects of the heat baths and at low temperatures due to quantum effects. Notably, the inset of Fig. 1 shows that α displays continuous behavior, with a pronounced valley observed in phases E and HO. In phase E, the maximum $|\xi|$ exceeds 0.3, whereas in phase HO, ξ remains nearly zero. At high temperatures, the size effects of the heat baths and the coupling between the quantum system and the bath becomes negligible, resulting in α approaching 1. In the inset of Fig. 1, we focus on the behaviors of $\alpha - t$ at low temperatures while the high-temperature regime is omitted. At high temperatures, both the system and the bath exhibit classical behavior as $\alpha \to 1$. The five distinct phases arise from different critical behaviors of α. The plots of f^*_tot as a function of α under specific parameters are shown in Fig. 2, illustrating these critical behaviors with black and green arrows driven by temperature at particular values of N_b and c_s, as well as by finite size and system-bath coupling effects, respectively. These plots provide schematic representations of how α sharply changes as a function of T and certain parameters, to maintain the minimum of f^*_tot.

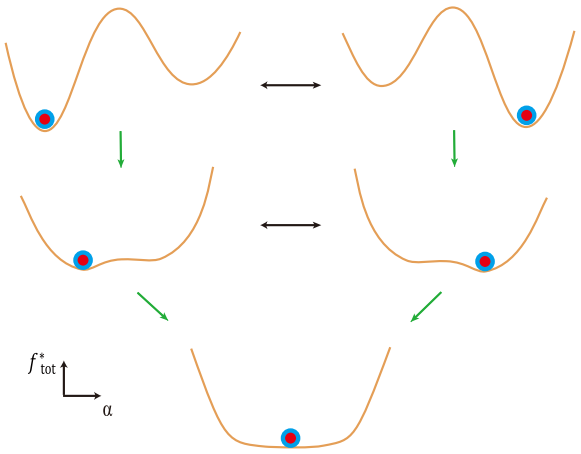

FIG. 2. The graphical representation of f^*_tot as a function of α illustrates the critical behavior of α concerning temperature and system parameters across different phases. The total system comprises the system of interest (depicted as a solid red circle) and its surrounding heat bath (shown as blue circles). The free energy density double-well landscapes are characterized by two states: the L-state ($\alpha \sim 0$) on the left and the R-state ($\alpha \sim 1$) on the right. The left-pointing black arrows indicate the transition of the total system from the L-state to the R-state as the temperature increases beyond T_L. Conversely, the right-pointing arrows represent the reverse transition at a lower temperature T_R. The green arrow in the right and the left plane represents the process of R-fusion and L-fusion, respectively, where the two minima in the free energy landscape within phase D merge into a single, flatter minimum at T_R and T_L.

The free energy landscape features the R-state (with $\alpha \sim 1$) on the right and the L-state (with $\alpha \sim 0$) on the left. Among the five singular phases, we observe rapid changes in α at critical points, denoted as T_L and T_R. The system stabilizes in the state corresponding to the lower of the two minima of f^*_tot. Transitions between the R- and L-states are indicated by bidirectional black arrows, representing jumps at T_R and T_L, defined as R jump and L jump, respectively. Fusion of the R- and L-states is marked by green arrows: R-fusion at T_R and L-fusion at T_L. These critical behaviors can lead to valleys, peaks, and even jumps in entropy and specific heat. The first type of critical behavior at T_R is primarily due to the finite-size effects of the baths, while the second type at T_L is driven by system-bath coupling effects. As N_b increases, the transition from phase D to phase E is indicated by the R-jump changing

to R-fusion. Similarly, as c_s increases, L-fusion occurs in phase D and at the boundary between phases D and C. The transition from phase D to phase C is marked by L-fusion turning into an L-jump, despite the small barrier between L- and R-states. In phase C, the barrier increases with c_s, leading to bifurcation again. The transition to phase E-HO occurs when the L-state disappears, while the transition to phase C-HO happens when the R- and L-states degenerate at a critical temperature, with the system initially in the R-state. Beyond this point, the system stabilizes in the R-state. In phase HO, the system remains in the R state across all temperatures. The behaviors of phases A and B are discussed in Sec. IV.

IV. RESULTS

Now, we discuss how the different dependencies of α on temperature lead to various even singular behavior in thermodynamic quantities in detail. From Eq. (18b) we known $Z_s^* = Z_s \delta Z_s^*$ where $Z_s = 1/(2\sinh\frac{1}{2}\beta\Omega)$ is the partition function for the bare HO with $N_s = 1$, and $\delta Z_s^* = 1/\sqrt{1+y_s}$ is the quantum correction on the partition function due to the noncommutativity of operators arising from the coupling between the system and the finite heat bath. Substituting this Z_s^* into Eqs. (7) and (8) for $\nu = s$, one has the formula for entropy, internal energy, and specific heat in the form

$$Q_s^* = Q_s + \delta Q_s^* \tag{21}$$

with the bare Q_s and its quantum correction δQ_s^*. For entropy S_s^*, we have $S_s = \frac{1}{2}\beta\Omega\coth\frac{1}{2}\beta\Omega - \ln(2\sinh\frac{1}{2}\beta\Omega)$ with $N_s = 1$ and

$$\delta S_s^* = -\frac{1}{2}\ln(1+y_s) - \frac{1}{2}\frac{\zeta_s}{1+y_s}, \tag{22}$$

where $\zeta_s = T\frac{\partial y_s}{\partial T}$ is the dimensionless slope of y_s with respective to T. Note that α is a function of (T, N_b, c_s, ω_D), and y_s is a function of (T, α). Therefore from Eq. (10) we have

$$\begin{aligned}\zeta_s &= T\left(\frac{\partial y_s}{\partial T}\right)_\alpha + \xi\left(\frac{\partial y_s}{\partial \alpha}\right)_T \\ &= \left(-1 + \frac{\beta\Omega}{\sinh\beta\Omega} - \frac{2\xi}{1-\alpha}\right)y_s,\end{aligned} \tag{23}$$

with $\xi = T\frac{\partial\alpha}{\partial T}$ being the dimensionless slope of α with respective to T. For internal energy E_s^*, we have $E_s = \frac{1}{2}\Omega\coth\frac{1}{2}\beta\Omega$ and $\delta E_s^* = -\frac{1}{2}\frac{\zeta_s T}{1+y_s}$. From this internal energy formula, we have the specific heat $C_V^* = C_V + \delta C_V^*$ with $V = V_s$, where bared $C_V = \frac{1}{4}\beta\Omega\sinh^{-2}\frac{1}{2}\beta\Omega$, and its correction

$$\begin{aligned}\delta C_V^* = &\frac{\zeta_s}{1+y_s}\left[\frac{\zeta_s}{2(1+y_s)} - \frac{\beta\Omega}{2\sinh\beta\Omega} + \frac{\xi}{1-\alpha}\right] \\ &+ \frac{y_s}{1+y_s}\left[\frac{\beta\Omega(1-\beta\Omega\coth\beta\Omega)}{2\sinh\beta\Omega} + \left(\frac{\xi}{1-\alpha}\right)^2\right. \\ &\left.+ \frac{\xi + T^2\partial^2\alpha/\partial T^2}{1-\alpha}\right].\end{aligned} \tag{24}$$

Then the rich properties are calculated by these explicit expressions.

Firstly, in phases A and B, $\alpha \to 0$ as the temperature approaches zero, shown in the inset of Fig. 1, which contrasts with the traditional limit where $\alpha \to 1$. The entropy and specific heat do not approach zero at zero temperature in these phases. For $y_s \simeq c_s\beta\Omega \to \infty$ and $\zeta_s \simeq -y_s \to -\infty$ as $T \to 0$, Eq. (22) gives $s_s^* = S_s^*/N_s k_B \simeq -\frac{1}{2}\ln c_s\Omega/T$, the entropy exhibits a logarithmic divergence at $T = 0$. Meanwhile, the specific heat tends toward $1/2$ at $T \to 0$ [44]: From Eq. (24), we have $c_V^* = C_V^*/N_s k_B \simeq [\zeta_s/(1+y_s)]^2/2 \simeq 1/2$. This behavior contradicts the third law of thermodynamics. From a quantum mechanical point of view, the dispersion of the position $\langle Q^2\rangle \to 0$. Therefore, they are the nonphysical regimes in which the system stays in one place at zero temperature without any quantum fluctuations. Hence, the form of the thermal equilibrium state is inappropriate in regions where both c_s and N_b are small in phases A and B. In principle, it is valid for computing the partition function of distinguishable particles with arbitrary values of (N_s, N_b) using Eq. (18b). For indistinguishable particles, the exact partition function within canonical statistics is provided in a recurrent relation with given values of (N_s, N_b), as appeared in [43]. On the other hand, at phase A for enough small values of N_b and c_s, the small system statistics give a characteristic temperature T_0 (in order of the ground state energy), and all thermodynamic quantities vanish at $T \leqslant T_0$. Furthermore, phase A needs a generalized statistical factor $(1-\sigma\beta\hat{H}_s^*)^{1/\sigma}$ with $\sigma = 1/(N_b - 2)$ for $N_b > 2$ in 1D HO [45]. The exact partition function has been obtained in [43].

In phase C, as depicted in Fig. 3, $\alpha(T)$ exhibits two jump discontinuities indicating the occurrence of critical behaviors. The occurrence temperature of the first discontinuity denoted as T_R, is due to the system transitioning from the R-state to the L-state. This is characterized by $\alpha(T_R^+) - \alpha(T_R^-) < 0$, indicating that the one-sided limit from the positive direction is larger than that from the negative direction. The second discontinuity occurs at T_L, where the system transitions from the L-state to the R-state, characterized by $\alpha(T_L^+) - \alpha(T_L^-) > 0$. We consider two points: C1 within phase C and C2 at the boundary of phases D and C. At T_L, the entropy at C1 shows only a jump, whereas, at C2, it exhibits a peak due to the L-fusion, causing the specific heat to peak at T_L^- and dip into a valley at T_L^+, rather than displaying jumps at T_L.

In phase D, as shown in Fig. 4, as N_b increases, T_R rises, and the difference $\alpha(T_R^+) - \alpha(T_R^-)$ decreases, eventually leading the system into phase E. Near the boundary between phases C and E within phase D, points D1 and D2 in Fig. 4 exhibit distinct behaviors at T_R and T_L. At T_R, $\alpha(T)$ shows discontinuities at both D1 and D2. At D1, this causes a sharp jump and subsequent jump in the entropy s_s^*, and the specific heat c_V^* exhibits a jump. In contrast, at D2, the discontinuities at T_R are accompanied by a peak in $\xi(T)$, leading to a subsequent dip in the entropy s_s^* and a more complex pattern in c_V^*, characterized by additional peaks and valleys. At T_L, the behavior also diverges between D1 and D2. At D1, α increases rapidly, marked by a peak in $\xi(T)$, resulting in a pair of peaks and valleys in c_V^*. As N_b increases, the rise of α becomes more gradual, leading to smoother, more regular behavior in s_s^* and c_V^* near T_L at D2.

In phase E, Fig. 5(a) shows that α is a smooth function of T. The characteristic quantity ξ is displayed in the inset

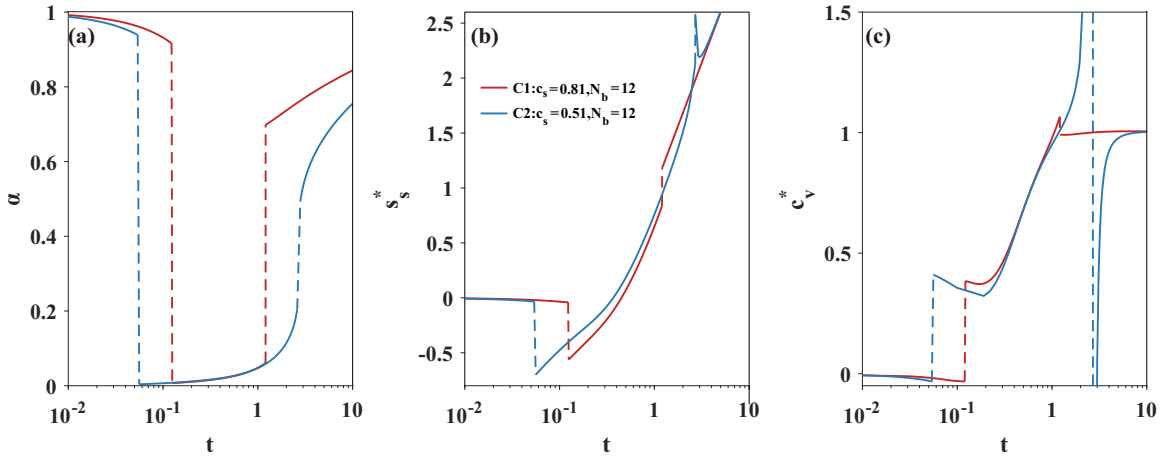

FIG. 3. Plots of (a) α, (b) entropy $s_s^* = S_s^*/N_s k_B$, and (c) specific heat $c_V^* = C_V^*/N_s k_B$ in phase C as a function of reduced temperature $t = T/\Omega$ using a base-10 logarithmic scale. We choose two points of the phase diagram at C1 with $c_s = 0.81$ and C2 with $c_s = 0.51$. We take $N_b = 12$ and $\bar{\omega}_D = 1000$.

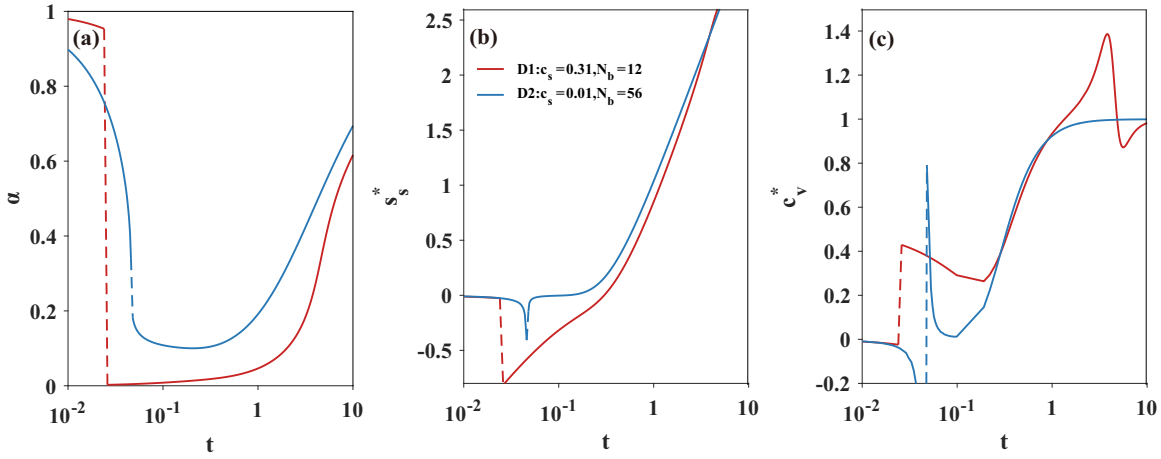

FIG. 4. Plots of (a) α, (b) s_s^*, and (c) c_V^* as a function of t in phase D, where t is on a base 10 logarithmic scale. We choose two points of the phase diagram at D1 with $c_s = 0.31$, $N_b = 12$ and D2 with $c_s = 0.01$, $N_b = 56$, and take $\bar{\omega}_D = 1000$.

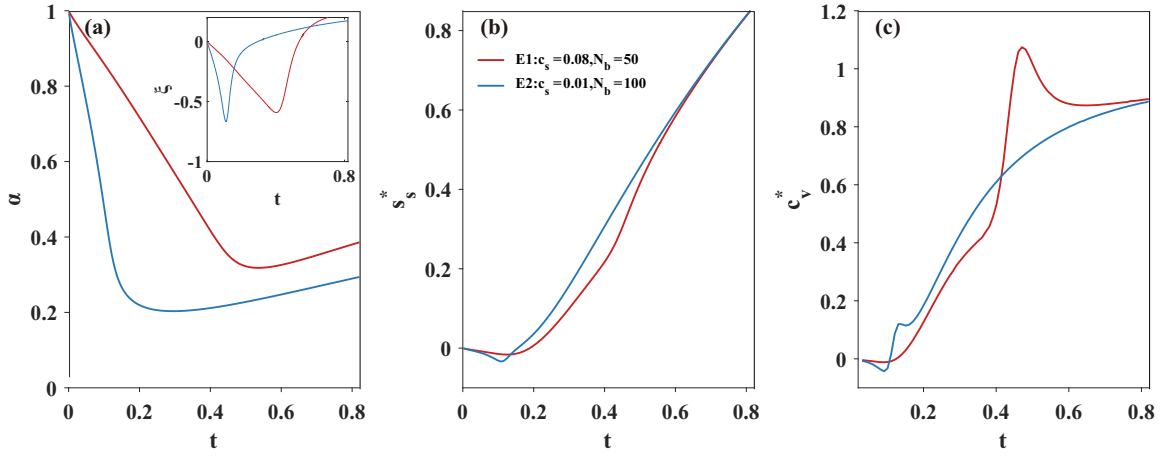

FIG. 5. Plots of (a) α, (b) s_s^*, and (c) c_V^* as a function of t in phase E. We choose two points of the phase diagram at E1 with $N_b = 50$, $c_s = 0.08$, and E2 with $N_b = 100$, $c_s = 0.01$. We take $\bar{\omega}_D = 1000$. Inset of (a) shows the curves of ξ vs t at points E1 and E2.

of Fig. 5(a). Notably, the singular phenomena in entropy and specific heat (valleys and peaks) at T_R in phase E, depicted in Figs. 5(b) and 5(c), are characterized not by the behavior of $\alpha(T)$, but by $\xi(T)$. Specifically, near the HO regime, where $\alpha \sim 1$ and $\xi \sim 0$, s_s^* and c_V^* exhibit smooth curves as functions of T, resulting in a smooth transition from phase E to phase HO.

It's worth noting that the phase HO can be accessed either by setting $c_s \gg 1$ or by significantly increasing N_b. In the TL, the coupling has little effect on the states of the heat bath. Therefore, by applying a semi-classical approximation, the partition function of the system becomes that of bare harmonic oscillators [24]. Interestingly, as $c_s \gg 1$, the system enters the phase HO, exhibiting characteristic behaviors consistent with free harmonic oscillators, which aligns with the results of [46]. However, [4] identifies a structural difference in the Gibbs factors of the state under strong coupling compared to the Gibbs state described in [46]. In [4], the system Hamiltonian is diagonalized in the interaction basis, whereas in [46], the Gibbs state of the system is diagonalized in the interaction basis under ultra-strong coupling, verified using hierarchical equations of motion. Notably, while both studies agree on a single qubit system, they diverge when the system is a harmonic oscillator. Our results align more closely with [46] and are further consistent with the quantum Zeno effect, which indicates that strong coupling suppresses heat exchange between the system and bath [46–48].

It is emphasized that the novel thermodynamic behaviors originate from the various dependencies of α on temperature due to the finite-size effects of the baths, causing the thermodynamic quantities defined through thermodynamic relations Eq. (7), Eq. (8), and formula Eq. (10). The singularity in entropy arises from δS_s^* which is determined by the values of α and ξ at fixed (T, N_b, c_s, ω_D). When parameters are chosen far from the boundary of phase D, the curve of ξ vs T lacks extreme except for discontinuities. Consequently in phases C and D, the thermodynamic quantities exhibit discontinuities due to different α values across the critical temperature, without showing peaks and valleys. However, near the boundary of phase D, the curve of ξ vs T features extremes: valleys near T_R and peaks near T_L. Consequently, S_s^* exhibits either a valley or an inflection point, leading to paired peaks and valleys in the specific heat. This behavior is observed in the thermodynamic quantities at points C2, D1, D2, E1, and E2.

Finally, the results reveal that entropy and specific heat exhibit diverse behaviors at the critical temperatures T_R and T_L, where T_R is less than 1. Figure 6 shows how these critical temperatures vary with typical values of N_b and changing c_s, incorporating the behaviors of $\alpha(T)$ and $\xi(T)$. We identify three typical phase transitions: D-C-HO, D-E-HO, and E-HO. As N_b increases above approximately 30, T_L disappears, because as c_s increases, the D $\rightarrow$ E transition replaces the D $\rightarrow$ C transition. Considering the effects of the system-bath coupling, there exists a maximum value of c_s for each N_b, referred to as the ultrastrong coupling point (UCP). Beyond this point, the system enters the HO phase, and critical temperatures are no longer observed [46–48]. The UCP gradually diminishes and eventually disappears as N_b increases. At the UCP, the behavior of the joint free energy density changes with two kinds of transitions. In the C-HO transition, T_R and T_L vanish

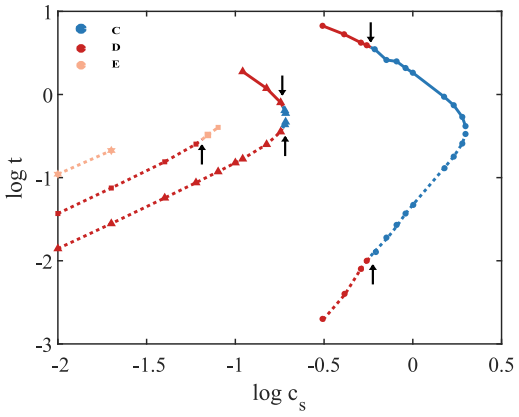

FIG. 6. Phase diagram of the critical temperature (sharp change occurs in the thermodynamic quantity) vs the effective coupling strength c_s with different N_b in a base-10 logarithmic scale on two coordinate axes ($\bar{\omega}_D = 1000$). Each curve consists of three elements: colors, line-styles, and markers. Three colors of blue, red and orange indicate three phases of C, D, and E. The lower T_R curves are shown in dotted lines, while higher T_L are shown in solid lines with the colors showing in the corresponding phase. The data points with circles, triangles, squares, and hexagons represent $N_b = 10, 30, 50,$ and 100, respectively, indicating the different phase transitions of D-C-HO, D-E-HO, and E-HO (the critical temperatures within this small c_s are not shown in phase A). These phase transition points are marked by the upward(downward) black arrows at the same critical points $T_R(T_L)$ between two phases. Note that the critical temperature in phase HO doesn't exist for the smooth curve of α vs T in large values c_s and arbitrary N_b.

at an intersection point, indicating that the R-state and L-state become degenerate. In the E-HO transition, the R-fusion does not occur, and the system remains in the R-state.

V. DISCUSSION

When the size of the bath is comparable to that of the system, it competes with the system for interactions, as a consequence of the diverse behaviors of $\alpha(T)$ using QHMFs. These behaviors are attributed to the presence of two local minimum points, called L-state and R-state in the reduced total free energy density f_{tot}^*. When comparing these two states and determining the minimum, we gain insights into the total system's stable state. As the temperature increases beyond a critical value, the minimum point undergoes a sudden transition, instigating a shift in the system's stable state from one to another leading to various peculiar phases. So both quantum effects and finite-size bath effects are clearly at play. At low temperatures, quantum effects and size considerations jointly determine α, while at high temperatures, α is almost 1 because the thermal energy dominates. In phases A and B, where the bath size is small, the third law of thermodynamics is violated due to the inappropriate form of the thermal equilibrium state, governed instead by a generalized statistical factor. Under weak coupling, the system's density of states is altered by the finite size effect of the heat baths, placing the system in either phase D or phase E. With stronger coupling, the system transitions to phase C, driven by the interaction between the quantum system and the baths. A UCP exists that decreases

with the increasing size of the bath. Beyond the UCP, the coupling effect is completely suppressed by the quantum Zeno effect, where α remains close to 1 and becomes largely insensitive to temperature.

To analytically solve the CL model within finite sizes, we employ a semi-classical approximation to obtain the result of the numerator in Eq. (16a). However, due to the system-bath coupling, we treat the system and the bath as each being the effective "bath" of the other, analogous to the concept of a bath in HMF. We then incorporate the quantum effect of this 'bath' on the system in the form of the Boltzmann factor, equivalent to applying the quantum correction in the statistical view. In our approach, the results in the TL closely resemble those of a bare harmonic oscillator, consistent with classical HMF in [24]. In contrast to the behavior of bare harmonic oscillators observed in our TL results, previous studies have reported different thermodynamic characteristics in continuous baths at low temperatures. For frequency-independent damping [27], c_V^* is given by $\pi T\gamma/3\Omega^2$ in leading order, applicable only under weak coupling. For a Drude model with frequency-dependent damping [44], c_V^* exhibits a peak, which becomes more pronounced at near-zero temperatures as c_s increases. These findings suggest that the combined size effects of finite heat baths and quantum effects at low temperatures contribute to the complex and varied behavior of α, leading to diverse phase diagrams and novel thermodynamic behaviors.

To experimentally study the finite bath size of a quantum system, we extend the setup from [37]. In insulator-ferromagnet-superconductor (I-F-S) layers, magnons are coupled to multiple superconducting (S) waveguides, which can be modeled using our discrete CL model. For simplicity, our peculiar phases can be observed with just ten modes in the bath, i.e., ten S waveguides. Given the magnon frequency in the GHz range, the critical temperatures of our model, as shown in Fig. 6, range from 10 μK to 50 mK, which is below the superconducting critical temperature. The coupling of the magnon to the jth photon is weighted by g_j, giving our effective coupling coefficient as $c_s = \sum_{j=1}^{N_b} \frac{2g_j^2}{\Omega\omega_j}$. This allows for designing photon frequencies to achieve c_s in the range of $[0.3, 2]$. Although $C_j \propto -g_j$, the sign does not affect our calculations. The peaks and valleys in the specific heat of the magnon are expected to be measurable at critical temperatures in the experiment.

VI. CONCLUSION

In this work, we developed a theoretical framework called QHMFs to analyze open quantum systems strongly coupled to finite baths. By introducing the parameter α within the range $[0, 1]$ due to the finite system and bath, we quantified α and $1-\alpha$ as the mutual distribution between the system and bath, treating each as the effective "bath" of the other. Our approach integrates the coupling effect into both using a statistical factor, with α capturing the influence of the finite bath. This parameter was determined by minimizing the joint total free energy density. We emphasize that α indeed does alter the states of the baths, allowing us to explore the system's behavior across different temperatures, coupling strengths, and bath sizes.

Our analysis, particularly within the CL model, shows that the temperature-dependent α with six distinct types of $\alpha(T)$ behavior leads to a complex and varied phase diagram. Our findings reveal the emergence of unique phenomena, characterized by two distinct types of novel behaviors at critical temperatures T_L and T_R. These transitions are marked by valleys, peaks, negative values, and even discontinuities in entropy and specific heat. Notably, in phases A and B, the system's entropy and specific heat do not approach zero as the temperature decreases, violating the third law of thermodynamics. This anomaly is attributed to the breakdown of equilibrium assumptions in regimes with few bath modes and weak coupling. In contrast, phases C, D, and E exhibit more complex behaviors, including entropy and specific heat discontinuities, as well as transitions between R-state and L-state at critical temperatures T_R and T_L. These findings highlight the significant influence of finite-size effects and quantum effects at low temperatures, leading to phenomena not observed in systems coupled to infinite baths. At high temperatures or with infinite baths, where $\alpha \to 1$, the theory reverts to classical behavior, consistent with the bare harmonic oscillator model. In the TL, the coupling does not affect the bath states, and the partition function Z_b^* aligns with that of bare harmonic oscillators, causing QHMFs to revert to the HMF.

The impact of a few bath modes will be explored using generalized statistical factors in future work. Additionally, other models, such as the Rabi model [49,50], impurities in the lattice [42], and systems with non-Gaussian baths [51], will be discussed elsewhere.

ACKNOWLEDGMENTS

This work is supported by the National Natural Science Foundation of China under Grants No. 12175040 and No. 12465009 and the State Key Programs of China under Grant No. 2017YFA0304204.

[1] A. S. Trushechkin, M. Merkli, J. D. Cresser, and J. Anders, Open quantum system dynamics and the mean force Gibbs state, AVS Quantum Sci. **4**, 012301 (2022).

[2] C. Jarzynski, Stochastic and macroscopic thermodynamics of strongly coupled systems, Phys. Rev. X **7**, 011008 (2017).

[3] U. Seifert, First and second law of thermodynamics at strong coupling, Phys. Rev. Lett. **116**, 020601 (2016).

[4] J. D. Cresser and J. Anders, Weak and ultrastrong coupling limits of the quantum mean force Gibbs state, Phys. Rev. Lett. **127**, 250601 (2021).

[5] P. Talkner and P. Hänggi, *Colloquium*: Statistical mechanics and thermodynamics at strong coupling: Quantum and classical, Rev. Mod. Phys. **92**, 041002 (2020).

[6] A. Rivas, Strong coupling thermodynamics of open quantum systems, Phys. Rev. Lett. **124**, 160601 (2020).

[7] M. Campisi, P. Talkner, and P. Hänggi, Thermodynamics and fluctuation theorems for a strongly coupled open quantum system: An exactly solvable case, J. Phys. A: Math. Theor. **42**, 392002 (2009).

[8] J. Anders, C. R. J. Sait, and S. A. R. Horsley, Quantum brownian motion for magnets, New J. Phys. **24**, 033020 (2022).

[9] D. Orgad, V. Oganesyan, and S. Gopalakrishnan, Dynamical transitions from slow to fast relaxation in random open quantum systems, Phys. Rev. Lett. **132**, 040403 (2024).

[10] P. J. Paulino, I. Lesanovsky, and F. Carollo, Large deviation full counting statistics in adiabatic open quantum dynamics, Phys. Rev. Lett. **132**, 260402 (2024).

[11] N. Lambert, Y.-N. Chen, Y.-C. Cheng, C.-M. Li, G.-Y. Chen, and F. Nori, Quantum biology, Nat. Phys. **9**, 10 (2013).

[12] A. Bachtold, J. Moser, and M. I. Dykman, Mesoscopic physics of nanomechanical systems, Rev. Mod. Phys. **94**, 045005 (2022).

[13] P. C. Burke, G. Nakerst, and M. Haque, Structure of the Hamiltonian of mean force, Phys. Rev. E **110**, 014111 (2024).

[14] J. Rosa and M. W. Beims, Dissipation and transport dynamics in a ratchet coupled to a discrete bath, Phys. Rev. E **78**, 031126 (2008).

[15] Q. Wei, S. T. Smith, and R. Onofrio, Equilibrium states of a test particle coupled to finite-size heat baths, Phys. Rev. E **79**, 031128 (2009).

[16] J. Nys, Z. Denis, and G. Carleo, Real-time quantum dynamics of thermal states with neural thermofields, Phys. Rev. B **109**, 235120 (2024).

[17] A. Riera-Campeny, A. Sanpera, and P. Strasberg, Open quantum systems coupled to finite baths: A hierarchy of master equations, Phys. Rev. E **105**, 054119 (2022).

[18] G. T. Landi, D. Poletti, and G. Schaller, Nonequilibrium boundary-driven quantum systems: Models, methods, and properties, Rev. Mod. Phys. **94**, 045006 (2022).

[19] P. Strasberg, G. Schaller, N. Lambert, and T. Brandes, Nonequilibrium thermodynamics in the strong coupling and non-Markovian regime based on a reaction coordinate mapping, New J. Phys. **18**, 073007 (2016).

[20] S. Genway, A. F. Ho, and D. K. K. Lee, Thermalization of local observables in small Hubbard lattices, Phys. Rev. A **86**, 023609 (2012).

[21] M. Panfil, S. Gopalakrishnan, and R. M. Konik, Thermalization of interacting quasi-one-dimensional systems, Phys. Rev. Lett. **130**, 030401 (2023).

[22] J. Wang, M. H. Lamann, J. Richter, R. Steinigeweg, A. Dymarsky, and J. Gemmer, Eigenstate thermalization hypothesis and its deviations from random-matrix theory beyond the thermalization time, Phys. Rev. Lett. **128**, 180601 (2022).

[23] T. L. Hill, A different approach to nanothermodynamics, Nano Lett. **1**, 273 (2001).

[24] M. F. Gelin and M. Thoss, Thermodynamics of a subensemble of a canonical ensemble, Phys. Rev. E **79**, 051121 (2009).

[25] H. Grabert, U. Weiss, and P. Talkner, Quantum theory of the damped harmonic oscillator, Z. Phys. B **55**, 87 (1984).

[26] B. L. Hu, J. P. Paz, and Y. Zhang, Quantum brownian motion in a general environment: Exact master equation with nonlocal dissipation and colored noise, Phys. Rev. D **45**, 2843 (1992).

[27] G. W. Ford and R. F. O'Connell, Quantum thermodynamic functions for an oscillator coupled to a heat bath, Phys. Rev. B **75**, 134301 (2007).

[28] M. Brenes, J. J. Mendoza-Arenas, A. Purkayastha, M. T. Mitchison, S. R. Clark, and J. Goold, Tensor-network method to simulate strongly interacting quantum thermal machines, Phys. Rev. X **10**, 031040 (2020).

[29] A. O. Caldeira and A. J. Leggett, Influence of dissipation on quantum tunneling in macroscopic systems, Phys. Rev. Lett. **46**, 211 (1981).

[30] A. J. Leggett, S. Chakravarty, A. T. Dorsey, M. P. A. Fisher, A. Garg, and W. Zwerger, Dynamics of the dissipative two-state system, Rev. Mod. Phys. **59**, 1 (1987).

[31] C. Kwon and J.-Y. Gyhm, Dynamics of a small quantum system open to a bath with thermostat, Phys. Rev. E **110**, 044141 (2024).

[32] U. Weiss, *Quantum Dissipative Systems*, 4th ed. (World Scientific, 2012).

[33] S. Hilt, B. Thomas, and E. Lutz, Hamiltonian of mean force for damped quantum systems, Phys. Rev. E **84**, 031110 (2011).

[34] P. Hänggi, G.-L. Ingold, and P. Talkner, Finite quantum dissipation: the challenge of obtaining specific heat, New J. Phys. **10**, 115008 (2008).

[35] S. S. Zhang, E. Berg, and A. V. Chubukov, Free energy and specific heat near a quantum critical point of a metal, Phys. Rev. B **107**, 144507 (2023).

[36] G. Bourcin, J. Bourhill, V. Vlaminck, and V. Castel, Strong to ultrastrong coherent coupling measurements in a YIG/cavity system at room temperature, Phys. Rev. B **107**, 214423 (2023).

[37] I. A. Golovchanskiy, N. N. Abramov, V. S. Stolyarov, A. A. Golubov, M. Y. Kupriyanov, V. V. Ryazanov, and A. V. Ustinov, Approaching deep-strong on-chip photon-to-magnon coupling, Phys. Rev. Appl. **16**, 034029 (2021).

[38] R. M. Fye, New results on Trotter-like approximations, Phys. Rev. B **33**, 6271 (1986).

[39] J.-T. Hsiang and B.-L. Hu, Quantum thermodynamics at strong coupling: Operator thermodynamic functions and relations, Entropy **20**, 423 (2018).

[40] P. Strasberg and A. Winter, First and second law of quantum thermodynamics: A consistent derivation based on a microscopic definition of entropy, PRX Quantum **2**, 030202 (2021).

[41] G. W. Ford, J. T. Lewis, and R. F. O'Connell, Quantum Langevin equation, Phys. Rev. A **37**, 4419 (1988).

[42] R. Bulla, H.-J. Lee, N.-H. Tong, and M. Vojta, Numerical renormalization group for quantum impurities in a bosonic bath, Phys. Rev. B **71**, 045122 (2005).

[43] J.-h. Wang and Y.-l. Ma, Thermodynamics and finite-size scaling of homogeneous weakly interacting Bose gases within exact canonical statistics, Phys. Rev. A **79**, 033604 (2009).

[44] G.-L. Ingold, P. Hänggi, and P. Talkner, Specific heat anomalies of open quantum systems, Phys. Rev. E **79**, 061105 (2009).

[45] H.-Y. Tang, J.-H. Wang, and Y.-L. Ma, A new approach for the statistical thermodynamic theory of the nonextensive systems confined in different finite traps, J. Phys. Soc. Jpn. **83**, 064004 (2014).

[46] K. Goyal and R. Kawai, Steady state thermodynamics of two qubits strongly coupled to bosonic environments, Phys. Rev. Res. **1**, 033018 (2019).

[47] A. Kato and Y. Tanimura, Quantum heat transport of a two-qubit system: Interplay between system-bath coherence and qubit-qubit coherence, J Chem Phys **143**, 064107 (2015).

[48] P. Rebentrost, M. Mohseni, I. Kassal, S. Lloyd, and A. Aspuru-Guzik, Environment-assisted quantum transport, New J. Phys. **11**, 033003 (2009).

[49] I. I. Rabi, On the process of space quantization, Phys. Rev. **49**, 324 (1936).

[50] G. De Filippis, A. de Candia, G. Di Bello, C. A. Perroni, L. M. Cangemi, A. Nocera, M. Sassetti, R. Fazio, and V. Cataudella, Signatures of dissipation driven quantum phase transition in Rabi model, Phys. Rev. Lett. **130**, 210404 (2023).

[51] L. J. Bond, A. Safavi-Naini, and J. Minář, Fast quantum state preparation and bath dynamics using non-Gaussian variational *Ansatz* and quantum optimal control, Phys. Rev. Lett. **132**, 170401 (2024).